


Time-reversal symmetry breaking from lattice dislocations in superconductorsClara N. Breið, ¹ Andreas Kreisel , ¹ Mercè Roig , ¹ P. J. Hirschfeld, ² and Brian M. Andersen ¹¹*Niels Bohr Institute, University of Copenhagen, DK-2200 Copenhagen, Denmark*²*Department of Physics, University of Florida, Gainesville, Florida 32611, USA* (Received 9 October 2023; revised 10 December 2023; accepted 18 December 2023; published 10 January 2024)

Spontaneous generation of time-reversal symmetry breaking in unconventional superconductors is currently a topic of considerable interest. While chiral superconducting order is often assumed to be the source of such signatures, they can sometimes also arise from nonmagnetic disorder. Here we perform a theoretical study of the impact of dislocations on the superconducting order parameter within a microscopic one-band model which, in the homogeneous case, features either extended s -wave, d -wave, or $s + id$ -wave superconductivity depending on the electron concentration. We find that the dislocations minimize their impact on the superconducting condensate by inducing localized supercurrents pinned by the dislocations, even well outside the $s + id$ regime. We map out the parameter and density dependence of the induced currents. From these results we conclude that quite generically unconventional superconductors hosting dislocations tend to break time-reversal symmetry locally.

DOI: [10.1103/PhysRevB.109.014505](https://doi.org/10.1103/PhysRevB.109.014505)**I. INTRODUCTION**

A growing class of unconventional superconductors have been discovered to exhibit evidence of spontaneous time-reversal symmetry breaking (TRSB) below their critical temperatures T_c [1,2]. This is evidenced, for example, by enhanced muon-spin relaxation (μ SR) and polar Kerr effect measurements reporting a change in the optical polar Kerr angle below T_c . This points to internal magnetic fields spontaneously generated by the superconducting state itself. A natural explanation for the occurrence of such fields would be either in terms of a nonunitary triplet pairing state or multicomponent superconducting condensates entering a TRSB by a complex superposition of the order. For superconducting instabilities condensing in two-dimensional (2D) irreducible representations of the associated crystal point group, the latter interpretation appears particularly appealing. Complex superpositions of two symmetry-distinct order parameters may exhibit persistent supercurrents at material edges, dislocations, or around various defect sites. The multicomponent scenario for the origin of TRSB below T_c has been extensively discussed for, e.g., Sr_2RuO_4 [3,4], and heavy-fermion compounds UPt_3 [5,6], UTe_2 [7,8], $\text{PrOs}_4\text{Sb}_{12}$ [9,10], and also for $\text{Ba}_{1-x}\text{K}_x\text{Fe}_2\text{As}_2$ [11,12], LaNiC_2 [13], and more recently additionally for the kagome superconductors AV_3Sb_5 (A : K, Rb, Cs) [14–16]. At present, however, the status of the precise superconducting ground state remains controversial for several of these materials (e.g., Sr_2RuO_4 and UTe_2), partly due to specific heat data featuring only a single transition that does not split under uniaxial strain.

Thus, it is important to pursue further possibilities for the origin of TRSB generated inside the superconducting phase. In particular, one might ask what mechanisms exist for TRSB for superconducting condensates composed of a single-component order parameter? The answer to this question necessarily involves the presence of spatial inhomogeneities.

For example, it is well known that nonmagnetic impurities can generate magnetic moments on nearby sites below T_c [17–30] in the presence of electronic correlations. In addition, one can envision disorder-induced slowing down of magnetic fluctuations of preexisting magnetic impurities, thereby lowering the characteristic fluctuation frequencies into the muon time window. Another possibility for TRSB includes the generation of localized orbital loops of supercurrents. The latter is well known to arise near nonmagnetic disorder sites in complex TRSB multicomponent condensates [31–38], but was recently shown to be also present in the strong disorder limit of single-component superconductors [39,40]. Likewise, one might expect dislocations and grain boundaries to similarly operate as seeds of localized loop currents. Recently, the latter scenario was proposed by Willa *et al.* [41], as a possible explanation for reconciling the existence of TRSB and a single specific heat transition in Sr_2RuO_4 . Indeed, for this material it is well known that dislocations are prevalent in many samples [42].

Here, motivated by the above-mentioned developments, we perform a detailed theoretical study of the possibility of generation of localized supercurrents by dislocations in single-component order parameter superconductors. For concreteness, we focus on a one-band model with nearest-neighbor attractive interactions. This model supports either B_{1g} (d -wave) or A_{1g} (extended s -wave) spin-singlet superconductivity in the homogeneous case, depending on filling. In addition, there exists a coexistence regime where the complex combination $s + id$ is favored. We start from a single-band picture without any material-specific details, except the assumption that the orbital states are of $d_{x^2-y^2}$ symmetry. To obtain the modifications of the hopping integrals due to a dislocation, we remove a line of l atoms and simulate the equilibrium positions assuming parabolic potentials between the atoms in a molecular dynamics setup. The hopping integrals

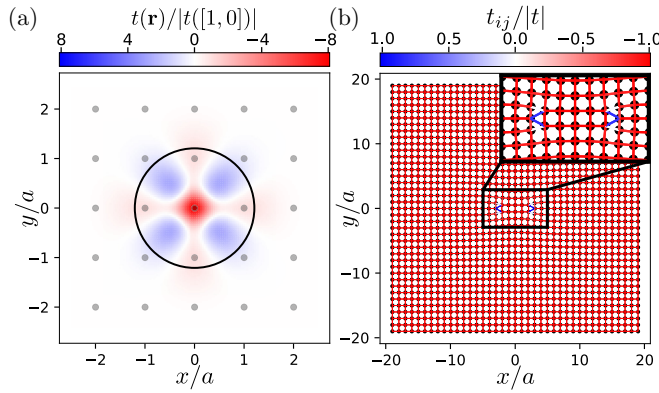


FIG. 1. (a) Hopping integral as function of connection vector \mathbf{r} between sites. Black circle shows $r_{\text{cut}} = (1 + \sqrt{2})/2$ defining the maximum distance allowed for NN bonds. Grey dots indicate site positions of the homogeneous lattice. (b) An example of real-space points (black dots) describing a $l = 5$ dislocation together with the value of the hopping integral (colored bonds). The inset shows a zoom-in of the region close to the dislocation.

are then the expectation value of the kinetic energy in atomlike $d_{x^2-y^2}$ orbitals separated by the distances determined in this manner. From selfconsistent real-space studies and associated calculations of the free energy, we find that the dislocations favor the local generation of complex pair potential order in a rather broad range of parameters and electron concentrations. This implies that TRSB dislocation-bound orbital currents are spontaneously stabilized. Our results highlight the role of spatial inhomogeneity in generating TRSB and associated magnetic signals within the superconducting phase.

II. MODEL AND METHOD

A. Dislocations and lattice relaxation

The normal-state Hamiltonian of a system of real-space points with hopping matrix elements t_{ij} is given by

$$H_0 = \sum_{i,j,\sigma} (t_{ij} - \mu\delta_{ij}) c_{i\sigma}^\dagger c_{j\sigma}, \quad (1)$$

where the operator $c_{i\sigma}^\dagger$ creates an electron at real-space point i with spin σ . For a homogeneous system, we set $t_{ij} = t = -1$ if i and j are nearest neighbors (NN). In the presence of a dislocation, the displacements of lattice points modifies the hopping integrals which we capture in the following way. Given the distance vector $\mathbf{r}_{ij} = (x_{ij}, y_{ij})$, we calculate the hopping from the expectation value $t(\mathbf{r}_{ij}) = \langle \psi_0 | -1/(2m)\nabla^2 | \psi_{\mathbf{r}_{ij}} \rangle$ of the kinetic energy $-1/(2m)\nabla^2$ for overlapping atomic $d_{x^2-y^2}$ wavefunctions $\langle \mathbf{r} | \psi_{\mathbf{r}_{ij}} \rangle$ centered at \mathbf{r}_{ij} . The result of this calculation for distances \mathbf{r} in the x - y plane is shown in Fig. 1(a). The effective mass m in the kinetic energy operator is chosen such that the value for the NN hopping is given by $|t([1, 0])| = 1$ as it was also used in Ref. [43]. Black circle shows $r_{\text{cut}} = (1 + \sqrt{2})/2$ defining the maximum distance allowed for NN bonds. Hopping amplitudes for $|\mathbf{r}_{ij}| > r_{\text{cut}}$ are simply set to zero in our calculation. Note that the implementation of a dislocation reduces the total number of sites in an $N \times N$ square lattice to $N^2 - l$.

The positions of the lattice points are obtained using a molecular dynamics simulation with periodic boundary conditions where the sites of a square lattice are bound to NN and next-nearest-neighbor (NNN) sites via unstretched strings of equal strength [43]. Next, a finite number l of lattice sites along a line are removed to form a dislocation pair and bonds to the “new” NN and NNN along that line are established. The relaxation under the harmonic potential (of the springs) with periodic boundary conditions is then done to find all positions \mathbf{r}_i of the lattice points. This procedure yields symmetric positions close to the dislocation and reproduces the strain expected from continuum theory far away from the dislocation. An example of the lattice positions (black dots) for $l = 5$ is shown in Fig. 1(b) where the value of the hopping integrals are indicated by the color of the corresponding bond.

B. Self-consistent solutions of superconductivity

The study presented here is based on the following one-band BCS mean-field Hamiltonian

$$H = H_0 - \sum_{(i,j)} [\Delta_{ij}(c_{i\downarrow}^\dagger c_{j\uparrow}^\dagger - c_{i\uparrow}^\dagger c_{j\downarrow}^\dagger) + \text{H.c.}], \quad (2)$$

where $\Delta_{ij} = V(\langle c_{j\uparrow} c_{i\downarrow} \rangle - \langle c_{j\downarrow} c_{i\uparrow} \rangle)$ is the attractive ($V > 0$) singlet pairing on NN bonds also defined by $|\mathbf{r}_{ij}| < r_{\text{cut}}$. The NN coupling can generate only two spin-singlet instabilities on the homogeneous 2D square lattice: the A_{1g} extended s -wave case with gap structure $\Delta(\mathbf{k}) = 2\Delta[\cos(k_x) + \cos(k_y)]$, and B_{1g} $d_{x^2-y^2}$ -wave superconductivity with gap structure $\Delta(\mathbf{k}) = 2\Delta[\cos(k_x) - \cos(k_y)]$. The corresponding Bogoliubov–de Gennes (BdG) equations are

$$E_n \begin{pmatrix} u_{in\downarrow} \\ v_{in\uparrow} \end{pmatrix} = \sum_j \begin{pmatrix} K_{ij} & 2\Delta_{ij} \\ 2\Delta_{ij}^* & -K_{ij} \end{pmatrix} \begin{pmatrix} u_{jn\downarrow} \\ v_{jn\uparrow} \end{pmatrix}, \quad (3)$$

where $u_{in\downarrow}$, $v_{in\uparrow}$ are the usual eigenvector components from the Bogoliubov transformation, $K_{ij} = t_{ij} - \mu\delta_{ij}$ and E_n are the eigenenergies of H . The equations are solved self-consistently for systems of size $N \times N$ with a dislocation of length l as described above. The convergence criterion is set to $|\mathcal{H}_{\alpha\beta}^s - \mathcal{H}_{\alpha\beta}^{s-1}| < 10^{-8} |t| \forall \alpha, \beta$, where \mathcal{H} is the BdG Hamiltonian and s denotes the iteration counter. All results are computed with open boundary conditions (OBC) to avoid supercell interference effects and we set $V = 0.75 |t|$ and $N \times N = 39 \times 39$ unless otherwise specified. Additionally, the average electron density will be fixed by adjusting the chemical potential μ in the self-consistent iterations. Results presented here are obtained for the hole-doped region of the phase diagram $\langle n \rangle < 1$, but applies also to the electron-doped region due to particle-hole symmetry at half-filling ($\mu = 0$) with the symmetry $\langle n \rangle \rightarrow 2 - \langle n \rangle$.

To study the possibility of spontaneous TRSB induced by the atomic dislocations and manifested by generation of orbital currents, the bond-current densities of all converged results are computed as

$$\begin{aligned} \langle j_{ij} \rangle &= -i \frac{e}{\hbar a^2} \sum_{\sigma} t_{ij} \langle c_{i\sigma}^\dagger c_{j\sigma} - c_{j\sigma}^\dagger c_{i\sigma} \rangle \\ &= 2 \frac{e}{\hbar a^2} \sum_n t_{ij} \text{Im} [u_{in\downarrow}^* u_{jn\downarrow} f(E_n) - v_{in\uparrow}^* v_{jn\uparrow} f(E_n)], \quad (4) \end{aligned}$$

where e denotes the electron charge and $f(E_n)$ is the Fermi-Dirac distribution function. All results are obtained with the temperature fixed at $T = 0.001 |t|$. The self-consistency ensures current conservation as confirmed by incoming and outgoing currents being equal in magnitude at all lattice sites [44]. We project the bond-current densities to local densities using

$$\mathbf{j}_i = \frac{1}{2} \sum_{(i,j)} \frac{\langle j_{ij} \rangle}{|\mathbf{r}_{ij}|} \begin{pmatrix} x_{ij} \\ y_{ij} \end{pmatrix}. \quad (5)$$

C. Free energy calculation

Introducing spatial inhomogeneities in the self-consistent solution of the model vastly extends the parameter space in which the free energy should be minimized. As the self-consistency only ensures results to be at stationary points in the free-energy landscape, an enhancement of parameter space also increases the risk of obtaining converged results which do not represent the global minimum. Thus, to ensure that the spontaneous TRSB and generation of local loop currents are indeed energetically favorable, we compare the free energy of converged configurations with and without TRSB. The latter is obtained by restricting the superconducting order parameters to take real values at all bonds throughout the system. In this context, it should be noted that while Eq. (2) is written in the grand canonical ensemble we compare solutions with fixed particle number. Thus, the relevant quantity to consider is the free energy rather than the grand potential, i.e., $F = \Omega + \mu \langle \hat{N} \rangle$, where Ω is the grand potential and $\hat{N} = \sum_{i\sigma} c_{i\sigma}^\dagger c_{i\sigma}$. In the zero-temperature limit, this can be obtained as $F = \langle H \rangle + \mu \langle \hat{N} \rangle$ yielding simply

$$F = \sum_{(i,j),\sigma} t_{ij} \langle c_{i\sigma}^\dagger c_{j\sigma} \rangle - \sum_{(i,j)} \frac{|\Delta_{ij}|^2}{V}, \quad (6)$$

where the expectation value is calculated using the eigenvalues E_n and eigenvector components $u_{in\downarrow}, v_{in\uparrow}$ of the Hamiltonian Eq. (2). Note that the constant term originating from the mean-field decoupling of the interactions which is not included in Eq. (2) cancels the contribution from the expectation value of one of the superconducting pairing terms.

III. RESULTS

A. Homogeneous phase diagram

To establish a baseline for the results obtained for systems with dislocation defects, the phase diagram for the homogeneous system as a function of electron density is shown in Fig. 2. The magnitude of the A_{1g} (extended s -wave, red line) and B_{1g} ($d_{x^2-y^2}$, blue line) order parameters are shown on the left axis while the site-averaged free-energy difference $\overline{\delta F} = (F_{\Delta \in \mathbb{C}} - F_{\Delta \in \mathbb{R}})/N^2$ is indicated on the right axis (black line). Here F is computed according to Eq. (6) and the subscript indicates whether Δ_{ij} are free to take on any value ($\Delta \in \mathbb{C}$) or they are restricted to real values preventing currents from developing ($\Delta \in \mathbb{R}$). For electron densities close to half-filling, $\langle n \rangle = 1$, the A_{1g} solution is strongly disfavored due to the near alignment of the Fermi surface and line nodes, and therefore the self-consistent solution exhibits B_{1g} symmetry. On the

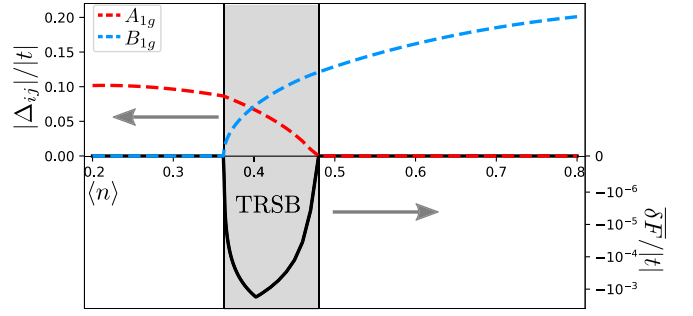


FIG. 2. Phase diagram showing on the left axis the amplitude of the homogeneous A_{1g} (extended s -wave, red line) and B_{1g} ($d_{x^2-y^2}$, blue line) order parameters as a function of electron density. The free-energy difference per site $\overline{\delta F} = (F_{\Delta \in \mathbb{C}} - F_{\Delta \in \mathbb{R}})/N^2$ is displayed on the right axis (black line). The results presented here are obtained by solving the self-consistency equations in momentum space using a k grid of 201×201 points.

contrary, for small Fermi pockets ($\langle n \rangle < 0.36$), a full gap can develop in the A_{1g} channel which is more favorable than the B_{1g} channel hosting four point nodes at the Fermi surface for all electron densities [38,45,46].

In the intermediate region $0.36 < \langle n \rangle < 0.48$, a complex superposition of the two channels is favored, yielding a TRSB solution of the form $A_{1g} \pm iB_{1g}$. A possible nematic solution $A_{1g} \pm B_{1g}$ exhibits line nodes at $k_x = \pm\pi/2$, while the TRSB solution reduces the line nodes to point nodes at $k_x = \pm k_y = \pm\pi/2$, resulting in a gain in condensation energy. This energy gain is reflected by the free-energy difference shown in black in Fig. 2. Note by the definition stated above, that a negative value of $\overline{\delta F}$ signifies a TRSB ground state. Pure A_{1g}/B_{1g} regions have $\overline{\delta F} = 0$, since the two solutions ($\Delta \in \mathbb{C}$ and $\Delta \in \mathbb{R}$) can only differ by a change in the global superconducting phase.

B. Loop currents and pairing modulations

Several earlier studies investigated the emergence of orbital currents induced by nonmagnetic defects in TRSB superconductors employing both phenomenological Ginzburg-Landau approaches and microscopic mean-field methods [31,33,34,39,40,47,48]. In particular, the studies reveal that superconductors with $A_{1g} + iB_{1g}$ pairing symmetries generate spontaneous supercurrents in the vicinity of various types of nonmagnetic potential scatterers, including pointlike and spatially extended impurities [33,40], system boundaries [31], as well as defects exhibiting nontrivial spatial structures [34]. While the dislocations introduced in this work do not act as simple potential scatterers, it is reasonable to assume that the spatial inhomogeneities also generate orbital localized currents in the $A_{1g} + iB_{1g}$ phase due to local fluctuations in the superconducting order parameter analogous to the results presented in previous studies [31,33,34,39,40,47,48]. Indeed, the computed self-consistent results for systems in the homogeneous TRSB density range including a dislocation in the center region confirm the formation of local loop currents surrounding the defect. We note that, while the specific current pattern and magnitude depend on the dislocation length, the

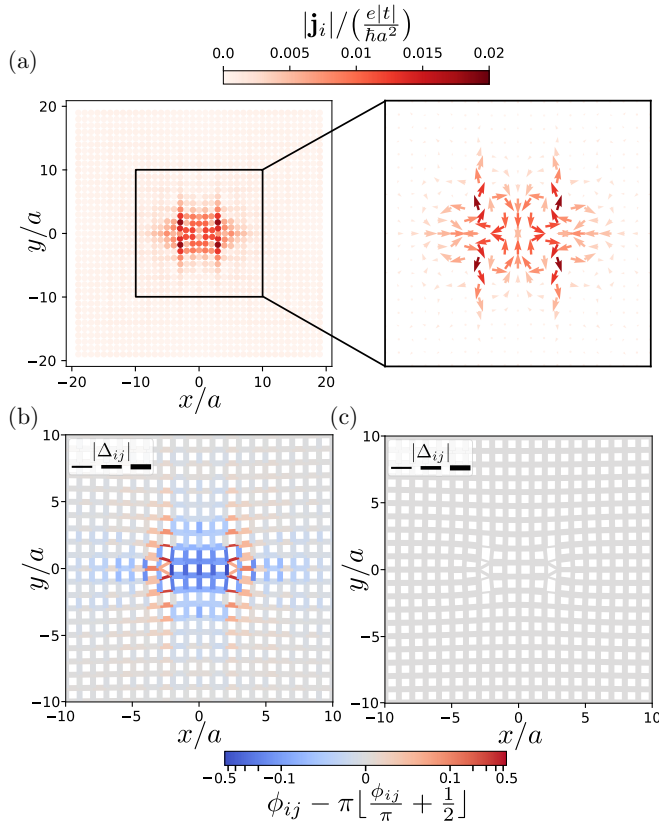


FIG. 3. (a) Site-resolved magnitude of the current density. Localized loop currents have developed near the dislocation with a small, long-range tail required by current conservation. Zoom-in shows the local current direction indicated by arrows. Arrow lengths have been rescaled for visual clarity. (b), (c) Modulations of Δ_{ij} for the converged solution with (b) and without (c) currents. Bond thickness indicates $|\Delta_{ij}|$ and bond color displays modulations of the bond phase, ϕ_{ij} . Here $\lfloor \cdot \rfloor$ is the floor function such that the nearest multiple of π is subtracted and only the deviations in ϕ_{ij} away from pure B_{1g} structure is shown. All results are computed with an $l = 5$ dislocation at $\langle n \rangle = 0.64$.

formation of currents is robust for all dislocations studied here.

While the generation of defect-induced supercurrents in the $A_{1g} + iB_{1g}$ phase might be expected, the emergence of currents in the pure A_{1g} or B_{1g} phases would require spontaneous TRSB occurring solely due to the lattice inhomogeneity associated with the presence of a dislocation. Surprisingly, we find that this scenario is indeed realized for a range of densities well within the homogeneous B_{1g} phase. This is unlike the property of single impurities which are unable to seed orbital currents in this region. Figure 3(a) displays the induced orbital currents for results obtained at $\langle n \rangle = 0.64$ and $l = 5$. The supercurrents are predominantly localized in the region extending ~ 5 lattice sites away from the dislocation, but current conservation requires a small, yet finite, long-range tail, see left panel of Fig. 3(a). The lack of corner/edge currents emphasizes that the near-homogeneous regions remain in the B_{1g} phase and, as such, the apparent breaking of TRS is a purely local and dislocation-induced effect. The zoom-in shown in the right panel displays the current direction, demonstrating

the orbital loops in the supercurrent pattern. The magnitudes are indicated by arrow color, while the arrow lengths have been rescaled for visual clarity.

Since supercurrents arise from modulations in the phase and amplitude of the order parameter, we display the bond-order parameters corresponding to Fig. 3(a) in Fig. 3(b). For comparison, Fig. 3(c) shows the converged result for identical parameters with the $\Delta_{ij} \in \mathbb{R}$ restriction applied (i.e., no currents allowed). The line thickness indicates the amplitudes of the bond pairings while the color displays the phase deviation away from $\phi_{ij} = 0, \pm\pi$, i.e., the deviation of the superconducting phase away from a pure B_{1g} phase with, e.g., $\phi_{ij} = 0$ on x bonds and $\phi_{ij} = \pi$ on y bonds. The restriction applied to the result shown in Fig. 3(c) obviously hinders phase modulations and the spatial inhomogeneity associated with the dislocation mainly serve as a pair-breaking effect as evident from the smaller gap amplitude on the bonds near the ends. In contrast, the current-carrying solution shown in Fig. 3(b) features clear deviations from the pure B_{1g} phase up to 18% as well as amplitude modulations similar to Fig. 3(c). Explicit comparison of the free-energy difference per site in this particular case yields indeed a negative $\delta\bar{F} = -2.4 \times 10^{-6}|t|$. This is much smaller than the typical reduction of the free energy when a homogeneous $A_{1g} + iB_{1g}$ state emerges; again a signature of the local nature of TRSB in this scenario.

C. Dislocation phase diagram and re-emerging supercurrents

Given the rather unexpected finding of energetically favorable loop currents far inside the homogeneous B_{1g} phase, it is desirable to perform a more extensive study of this phenomenon as a function of dislocation length and electron density. Thus, in Fig. 4 the left axis shows site-averaged supercurrent (dashed lines, circle markers) for dislocation lengths ranging from $l = 1$ to $l = 10$ as a function of density. As a direct reference to the phase diagram in Fig. 2, the homogeneous TRSB region has been marked in grey. It is evident that all dislocation lengths induce currents within this region as anticipated from the previous studies discussed above. We note, however, that the dome emerging from the homogeneous TRSB region is significantly enhanced with the upper phase boundary shifted from $\langle n \rangle = 0.48$ to $\langle n \rangle \sim 0.53$.

More interestingly, the generation of loop currents is clearly extended far beyond this main dome with re-emerging TRSB domes ranging all the way to $\langle n \rangle \sim 0.7$. While the density ranges and current strengths of the TRSB domes varies for different dislocation lengths, the multidome feature is universal across all systems investigated here, where some show an additional shoulder at the edge of the main dome (e.g., $l = 9$, marked in orange) and other show clearly distinguishable domes (e.g., $l = 2$, marked in purple, or $l = 5$, marked in cyan).

Figure 4 also shows the free-energy gain (solid lines, triangle markers) associated with the generation of loop currents on the right axis verifying that the TRSB solution is energetically preferred with the exception of a few points with degenerate time-reversal symmetric and TRSB solutions down to the convergence criterion, see e.g., $l = 7$ (light green) at $\langle n \rangle = 0.68$. Note that the individual contri-

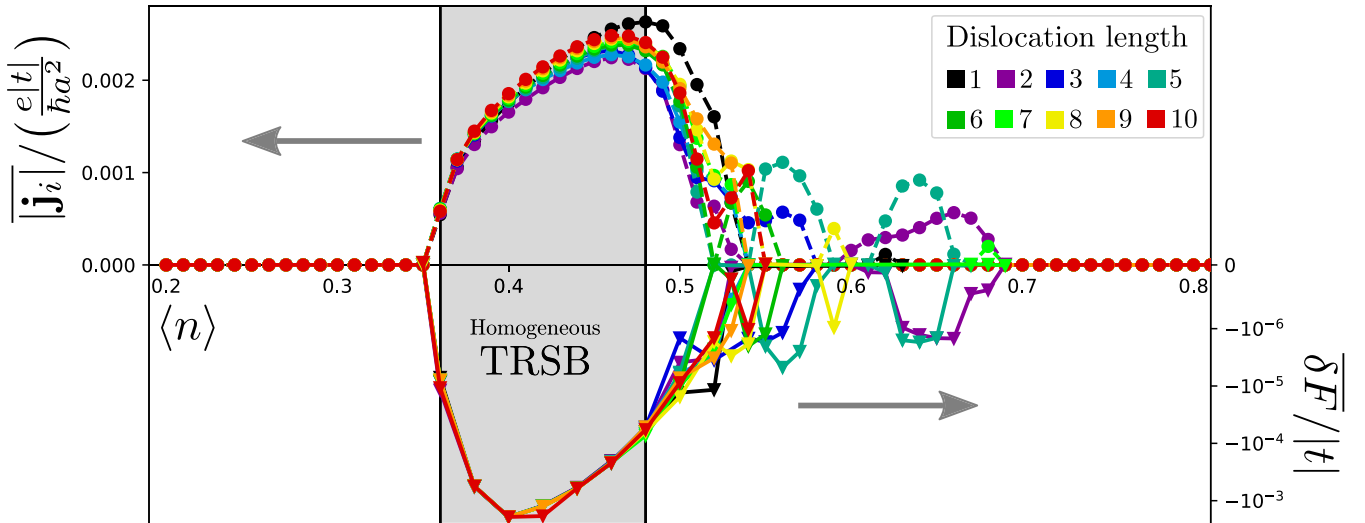


FIG. 4. Left axis: Site-averaged local current density magnitude (dashed lines, circle markers). A main TRSB dome extends from the homogeneous TRSB region (marked in grey) with re-emerging domes extending to $\langle n \rangle \sim 0.7$. Right axis: Site-averaged free energy gain (solid lines, triangle markers) associated with the spontaneous TRSB. All TRSB solutions are energetically favored or, in rare cases, degenerate with the time-reversal symmetric solution. Colors indicate different dislocation lengths l . Note that the total number of sites used in the averages is given by $N^2 - l$.

contributions from the two terms in Eq. (6) varies between loss and gain for different parameters and only the total free-energy difference reveal a consistent gain across all TRSB solutions.

IV. DISCUSSION AND CONCLUSIONS

It is relevant to highlight a fundamental difference between the spatial inhomogeneity introduced by dislocation defects and multiple impurities acting as dopants. Refs. [39,40] both found qualitatively similar results for strongly disordered systems ($>20\%$ dopant atoms) where spontaneous loop currents are formed well within the homogeneous B_{1g} phase. However, such strong disorder breaks all spatial symmetries and, as argued in Ref. [40], unavoidably introduce finite components of the other pairing symmetry channels. In contrast, the dislocation defects studied in this work preserve a global C_2 symmetry (C_4 symmetry for $l = 1$) around $\mathbf{r} = (0, 0)$ and, from a naive perspective, it is reasonable to assume that disorder with a higher symmetry should have less impact on the preferred symmetry of Δ_{ij} . However, as evident from the results presented here, the disorder does not need to be strong from a symmetry-breaking perspective to obtain TRSB ground states.

This is quite important, because many unconventional superconducting crystals are rather clean by many standard criteria, yet undoubtedly contain significant concentrations of such linear defects oriented by strain, which may be preferentially along high-symmetry axes. For example, the highest quality Sr_2RuO_4 crystals are famously extremely clean; tiny amounts of nonmagnetic disorder (e.g., 0.15% Ti^{4+} substituting for Ru^{4+}) suppress T_c to zero [49–51]. Both Kerr and μSR measurements indicate a small TRSB signal at the superconducting transition, yet the “standard” explanations in terms of two-component order parameters are seriously challenged by the absence of any splitting of the specific heat

transition with or without strain [52,53], suggesting alternative explanations for the weak TRSB. One such explanation was provided by Willa *et al.* [41], who assumed a close proximity of two pair components, d and g wave, such that a TRSB state was nucleated near an edge dislocation. Here we have demonstrated a similar scenario within a microscopic model, and also shown that the degeneracy need not be particularly close.

Additionally, apart from a few bonds located at the dislocation edges, all bonds exhibit near-homogeneous values of the hopping integrals leading to the expectation that a near-homogeneous B_{1g} phase should develop. To examine this in detail, we performed a systematic investigation of the amount of lattice distortion necessary to reproduce TRSB domes within the homogeneous B_{1g} phase and found within additional self-consistent calculations that even small modifications in the hopping integrals down to 5% must be included to *qualitatively* reproduce the results shown in Fig. 4. To *quantitatively* reproduce the results, all relaxation effects must be included. Furthermore, we have also found that the particular density ranges of nonzero currents and the associated current magnitudes shown in Fig. 4 varies a bit with system size (we have investigated a range of different systems up to 53×53 lattices) and boundary conditions (e.g., employing periodic boundaries). We stress, however, that the re-emergence of TRSB ground states within the homogeneous B_{1g} phase is a generic property not dependent on system size and boundary conditions. These combined findings suggest that the weak long-range perturbations and currents induced by the dislocation are essential. In this context, it is worth mentioning that typical dislocations in crystals may involve many hundreds of atoms, which presumably enhances these long-range effects.

In summary, we have performed a theoretical study of the preferred superconducting order near dislocations of a microscopic model that incorporates two symmetry-distinct

superconducting order parameters. It is found that dislocations tend to nucleate orbital currents and thereby locally break time-reversal symmetry spontaneously. This takes place even in regions of the phase diagram where the corresponding homogeneous superconducting condensate is single-component order. This effect may be important for the understanding of experiments reporting TRSB at T_c in unconventional superconductors.

ACKNOWLEDGMENTS

We acknowledge useful discussions with C. Hicks and M. Pal. C.N.B. and A.K. acknowledge support by the Danish National Committee for Research Infrastructure (NUFI) through the ESS-Lighthouse Q-MAT. P.J.H. acknowledges support from Grant No. NSF-DMR-1849751. M.R. acknowledges support from the Novo Nordisk Foundation Grant No. NNF20OC0060019.

-
- [1] S. K. Ghosh, M. Smidman, T. Shang, J. F. Annett, A. D. Hillier, J. Quintanilla, and H. Yuan, Recent progress on superconductors with time-reversal symmetry breaking, *J. Phys.: Condens. Matter* **33**, 033001 (2021).
- [2] H. S. Røising, G. Wagner, M. Roig, A. T. Rømer, and B. M. Andersen, Heat capacity double transitions in time-reversal symmetry broken superconductors, *Phys. Rev. B* **106**, 174518 (2022).
- [3] Y. Maeno, H. Hashimoto, K. Yoshida, S. Nishizaki, T. Fujita, J. G. Bednorz, and F. Lichtenberg, Superconductivity in a layered perovskite without copper, *Nature (London)* **372**, 532 (1994).
- [4] A. P. Mackenzie, T. Scaffidi, C. W. Hicks, and Y. Maeno, Even odder after twenty-three years: The superconducting order parameter puzzle of Sr_2RuO_4 , *npj Quantum Mater.* **2**, 40 (2017).
- [5] G. R. Stewart, Heavy-fermion systems, *Rev. Mod. Phys.* **56**, 755 (1984).
- [6] R. Joynt and L. Taillefer, The superconducting phases of UPt_3 , *Rev. Mod. Phys.* **74**, 235 (2002).
- [7] S. Ran, C. Eckberg, Q.-P. Ding, Y. Furukawa, T. Metz, S. R. Saha, I.-L. Liu, M. Zic, H. Kim, J. Paglione, and N. P. Butch, Nearly ferromagnetic spin-triplet superconductivity, *Science* **365**, 684 (2019).
- [8] D. Aoki, J.-P. Brison, J. Flouquet, K. Ishida, G. Knebel, Y. Tokunaga, and Y. Yanase, Unconventional superconductivity in UTe_2 , *J. Phys.: Condens. Matter* **34**, 243002 (2022).
- [9] E. D. Bauer, N. A. Frederick, P.-C. Ho, V. S. Zapf, and M. B. Maple, Superconductivity and heavy fermion behavior in $\text{PrOs}_4\text{Sb}_{12}$, *Phys. Rev. B* **65**, 100506(R) (2002).
- [10] Y. Aoki, A. Tsuchiya, T. Kanayama, S. R. Saha, H. Sugawara, H. Sato, W. Higemoto, A. Koda, K. Ohishi, K. Nishiyama, and R. Kadono, Time-reversal symmetry-breaking superconductivity in heavy-fermion $\text{PrOs}_4\text{Sb}_{12}$ detected by muon-spin relaxation, *Phys. Rev. Lett.* **91**, 067003 (2003).
- [11] M. Rotter, M. Tegel, and D. Johrendt, Superconductivity at 38 K in the iron arsenide $(\text{Ba}_{1-x}\text{K}_x)\text{Fe}_2\text{As}_2$, *Phys. Rev. Lett.* **101**, 107006 (2008).
- [12] J. Böker, P. A. Volkov, K. B. Efetov, and I. Eremin, $s + is$ superconductivity with incipient bands: Doping dependence and STM signatures, *Phys. Rev. B* **96**, 014517 (2017).
- [13] A. D. Hillier, J. Quintanilla, and R. Cywinski, Evidence for time-reversal symmetry breaking in the noncentrosymmetric superconductor LaNiC_2 , *Phys. Rev. Lett.* **102**, 117007 (2009).
- [14] Z. Guguchia, C. Mielke III, D. Das, R. Gupta, J.-X. Yin, H. Liu, Q. Yin, M. H. Christensen, Z. Tu, C. Gong, N. Shumiya, M. S. Hossain, T. Gamsakhurdashvili, M. Elender, P. Dai, A. Amato, Y. Shi, H. C. Lei, R. M. Fernandes, M. Z. Hasan *et al.*, Tunable unconventional kagome superconductivity in charge ordered RbV_3Sb_5 and KV_3Sb_5 , *Nat. Commun.* **14**, 153 (2023).
- [15] C. Mielke III, D. Das, J.-X. Yin, H. Liu, R. Gupta, Y.-X. Jiang, M. Medarde, X. Wu, H. C. Lei, J. Chang, P. Dai, Q. Si, H. Miao, R. Thomale, T. Neupert, Y. Shi, R. Khasanov, M. Z. Hasan, H. Luetkens, and Z. Guguchia, Time-reversal symmetry-breaking charge order in a kagome superconductor, *Nature (London)* **602**, 245 (2022).
- [16] A. T. Rømer, S. Bhattacharyya, R. Valentí, M. H. Christensen, and B. M. Andersen, Superconductivity from repulsive interactions on the kagome lattice, *Phys. Rev. B* **106**, 174514 (2022).
- [17] H. Tsuchiura, Y. Tanaka, M. Ogata, and S. Kashiwaya, Local magnetic moments around a nonmagnetic impurity in the two-dimensional t-J model, *Phys. Rev. B* **64**, 140501 (2001).
- [18] Z. Wang and P. A. Lee, Local moment formation in the superconducting state of a doped Mott insulator, *Phys. Rev. Lett.* **89**, 217002 (2002).
- [19] J.-X. Zhu, I. Martin, and A. R. Bishop, Spin and charge order around vortices and impurities in high- T_c superconductors, *Phys. Rev. Lett.* **89**, 067003 (2002).
- [20] Y. Chen and C. S. Ting, States of local moment induced by nonmagnetic impurities in cuprate superconductors, *Phys. Rev. Lett.* **92**, 077203 (2004).
- [21] B. M. Andersen, P. J. Hirschfeld, A. P. Kampf, and M. Schmid, Disorder-induced static antiferromagnetism in cuprate superconductors, *Phys. Rev. Lett.* **99**, 147002 (2007).
- [22] J. W. Harter, B. M. Andersen, J. Bobroff, M. Gabay, and P. J. Hirschfeld, Antiferromagnetic correlations and impurity broadening of NMR linewidths in cuprate superconductors, *Phys. Rev. B* **75**, 054520 (2007).
- [23] B. M. Andersen, S. Graser, and P. J. Hirschfeld, Disorder-induced freezing of dynamical spin fluctuations in underdoped cuprate superconductors, *Phys. Rev. Lett.* **105**, 147002 (2010).
- [24] M. Schmid, B. M. Andersen, A. P. Kampf, and P. J. Hirschfeld, d-Wave superconductivity as a catalyst for antiferromagnetism in underdoped cuprates, *New J. Phys.* **12**, 053043 (2010).
- [25] M. N. Gastiasoro, P. J. Hirschfeld, and B. M. Andersen, Impurity states and cooperative magnetic order in Fe-based superconductors, *Phys. Rev. B* **88**, 220509(R) (2013).
- [26] M. N. Gastiasoro, I. Paul, Y. Wang, P. J. Hirschfeld, and B. M. Andersen, Emergent defect states as a source of resistivity anisotropy in the nematic phase of iron pnictides, *Phys. Rev. Lett.* **113**, 127001 (2014).
- [27] M. N. Gastiasoro and B. M. Andersen, Local magnetization nucleated by non-magnetic impurities in Fe-based superconductors, *J. Supercond. Novel Magn.* **28**, 1321 (2015).
- [28] J. H. J. Martiny, M. N. Gastiasoro, I. Vekhter, and B. M. Andersen, Impurity-induced antiferromagnetic order in

- Pauli-limited nodal superconductors: Application to heavy-fermion CeCoIn₅, *Phys. Rev. B* **92**, 224510 (2015).
- [29] M. N. Gastiasoro, F. Bernardini, and B. M. Andersen, Unconventional disorder effects in correlated superconductors, *Phys. Rev. Lett.* **117**, 257002 (2016).
- [30] J. H. J. Martiny, A. Kreisel, and B. M. Andersen, Theoretical study of impurity-induced magnetism in FeSe, *Phys. Rev. B* **99**, 014509 (2019).
- [31] W.-C. Lee, S.-C. Zhang, and C. Wu, Pairing state with a time-reversal symmetry breaking in FeAs-based superconductors, *Phys. Rev. Lett.* **102**, 217002 (2009).
- [32] J. Garaud and E. Babaev, Domain walls and their experimental signatures in $s + is$ superconductors, *Phys. Rev. Lett.* **112**, 017003 (2014).
- [33] S. Maiti, M. Sigrist, and A. Chubukov, Spontaneous currents in a superconductor with $s + is$ symmetry, *Phys. Rev. B* **91**, 161102(R) (2015).
- [34] S.-Z. Lin, S. Maiti, and A. Chubukov, Distinguishing between $s + id$ and $s + is$ pairing symmetries in multiband superconductors through spontaneous magnetization pattern induced by a defect, *Phys. Rev. B* **94**, 064519 (2016).
- [35] M. Silaev, J. Garaud, and E. Babaev, Phase diagram of dirty two-band superconductors and observability of impurity-induced $s + is$ state, *Phys. Rev. B* **95**, 024517 (2017).
- [36] J. Garaud, M. Silaev, and E. Babaev, Thermoelectric signatures of time-reversal symmetry breaking states in multiband superconductors, *Phys. Rev. Lett.* **116**, 097002 (2016).
- [37] A. Benfenati, M. Barkman, T. Winyard, A. Wormald, M. Speight, and E. Babaev, Magnetic signatures of domain walls in $s + is$ and $s + id$ superconductors: Observability and what that can tell us about the superconducting order parameter, *Phys. Rev. B* **101**, 054507 (2020).
- [38] M. Roig, A. T. Rømer, P. J. Hirschfeld, and B. M. Andersen, Revisiting superconductivity in the extended one-band Hubbard model: Pairing via spin and charge fluctuations, *Phys. Rev. B* **106**, 214530 (2022).
- [39] Z.-X. Li, S. A. Kivelson, and D.-H. Lee, Superconductor-to-metal transition in overdoped cuprates, *npj Quantum Mater.* **6**, 36 (2021).
- [40] C. N. Breið, P. J. Hirschfeld, and B. M. Andersen, Supercurrents and spontaneous time-reversal symmetry breaking by nonmagnetic disorder in unconventional superconductors, *Phys. Rev. B* **105**, 014504 (2022).
- [41] R. Willa, M. Hecker, R. M. Fernandes, and J. Schmalian, Inhomogeneous time-reversal symmetry breaking in Sr₂RuO₄, *Phys. Rev. B* **104**, 024511 (2021).
- [42] Y. A. Ying, N. E. Staley, Y. Xin, K. Sun, X. Cai, D. Fobes, T. J. Liu, Z. Q. Mao, and Y. Liu, Enhanced spin-triplet superconductivity near dislocations in Sr₂RuO₄, *Nat. Commun.* **4**, 2596 (2013).
- [43] M. Pal, L. Bettmann, A. Kreisel, and P. J. Hirschfeld, Magnetic anisotropy from linear defect structures in correlated electron systems, *Phys. Rev. B* **103**, 245132 (2021).
- [44] B. M. Andersen, I. V. Bobkova, P. J. Hirschfeld, and Y. S. Barash, $0 - \pi$ transitions in Josephson junctions with antiferromagnetic interlayers, *Phys. Rev. Lett.* **96**, 117005 (2006).
- [45] A. Kreisel, A. T. Rømer, P. J. Hirschfeld, and B. M. Andersen, Superconducting Phase Diagram of the Paramagnetic One-Band Hubbard Model, *J. Supercond. Novel Magn.* **30**, 85 (2017).
- [46] A. T. Rømer, A. Kreisel, I. Eremin, M. A. Malakhov, T. A. Maier, P. J. Hirschfeld, and B. M. Andersen, Pairing symmetry of the one-band Hubbard model in the paramagnetic weak-coupling limit: A numerical RPA study, *Phys. Rev. B* **92**, 104505 (2015).
- [47] M. J. Graf, A. V. Balatsky, and J. A. Sauls, Local time-reversal-symmetry breaking in $d_{x^2-y^2}$ superconductors, *Phys. Rev. B* **61**, 3255 (2000).
- [48] G. Seibold, L. Benfatto, C. Castellani, and J. Lorenzana, Amplitude, density, and current correlations of strongly disordered superconductors, *Phys. Rev. B* **92**, 064512 (2015).
- [49] A. P. Mackenzie, R. K. W. Haselwimmer, A. W. Tyler, G. G. Lonzarich, Y. Mori, S. Nishizaki, and Y. Maeno, Extremely strong dependence of superconductivity on disorder in Sr₂RuO₄, *Phys. Rev. Lett.* **80**, 161 (1998).
- [50] N. Kikugawa, A. Peter Mackenzie, and Y. Maeno, Effects of in-plane impurity substitution in Sr₂RuO₄, *J. Phys. Soc. Jpn.* **72**, 237 (2003).
- [51] N. Kikugawa, A. P. Mackenzie, C. Bergemann, R. A. Borzi, S. A. Grigera, and Y. Maeno, Rigid-band shift of the Fermi level in the strongly correlated metal: Sr_{2-y}La_yRuO₄, *Phys. Rev. B* **70**, 060508(R) (2004).
- [52] K. Deguchi, Z. Q. Mao, and Y. Maeno, Determination of the superconducting gap structure in all bands of the spin-triplet superconductor Sr₂RuO₄, *J. Phys. Soc. Jpn.* **73**, 1313 (2004).
- [53] Y.-S. Li, N. Kikugawa, D. A. Sokolov, F. Jerzembeck, A. S. Gibbs, Y. Maeno, C. W. Hicks, J. Schmalian, M. Nicklas, and A. P. Mackenzie, High-sensitivity heat-capacity measurements on Sr₂RuO₄ under uniaxial pressure, *Proc. Natl. Acad. Sci. USA* **118**, e2020492118 (2021).